Available online at www.sciencedirect.com

ScienceDirect

journal homepage: www.elsevier.com/locate/he

DFT calculations for the electronic structure of alpha phase of $CsMgH_3$ as advanced hydrogen storage materials

A.H. Reshak [a,b,*]

[a] New Technologies – Research Centre, University of West Bohemia, Univerzitni 8, 306 14 Pilsen, Czech Republic
[b] Center of Excellence Geopolymer and Green Technology, School of Material Engineering, University Malaysia Perlis, 01007 Kangar, Perlis, Malaysia

ARTICLE INFO

Article history:
Received 15 October 2015
Received in revised form
8 November 2015
Accepted 25 November 2015
Available online 20 December 2015

Keywords:
Hydrogen storage
α-$CsMgH_3$
DFT
Electronic charge density

ABSTRACT

Detail analyzes to the electronic structure of magnesium based ternary metal hydrides containing alkali and alkaline-earth elements (α-$CsMgH_3$) is reported so as to justify its use as advanced hydrogen storage systems. Calculations based on full-potential method within several exchange correlation potentials are performed to gain a reliable results. It has been found that α-$CsMgH_3$ exhibits indirect band gap of about 2.3 eV (local density approximation -LDA), 2.6 eV (generalized gradient approximation -PBE-GGA), 2.9 eV (Engel-Vosko generalized gradient approximation - EVGGA) and 3.2 eV (recently modified Becke-Johnson potential -mBJ). The electronic band structure and the density of states reveal that at the energy regions around −5.0 eV and from −3.5 eV up to −2.0 eV the H-1s state hybridized with Mg-3s state to form a peak at around −5.0 eV and three peaks between −3.5 eV and −2.0 eV. The energy region from −2.0 eV up to Fermi level is originated by the interactions between H-1s and Mg-2p states. Thus, the interactions between the orbitals of H and Mg atoms leads to form strong covalent bonding between H and Mg atoms. The conduction bands are mainly originated from the empty states of Cs and partially from Mg-3s/2p states, while H-1s has insignificant contribution to the empty states. The chemical bonding were analyzed in term of charge density and charge transfer, we found that a charge transfer towards H atom occur. To gain further insight for deeply understanding the electronic structure, the optical dielectric functions are calculated based on the calculated band structure.
Copyright © 2015, Hydrogen Energy Publications, LLC. Published by Elsevier Ltd. All rights reserved.

Introduction

In the recent years the alkali and alkaline earth based complex hydrides were comprehensively investigated to explore their suitability and stability as hydrogen strong materials at moderate pressures and temperatures [1–7]. The search for novel hydrogen storage material is still desirable. The magnesium based metal hydrides considered as potential candidates as constituents for advanced hydrogen storage materials due to their light weight and low cost [8]. These materials have good volume efficiency for hydrogen storage

* New Technologies – Research Centre, University of West Bohemia, Univerzitni 8, 306 14 Pilsen, Czech Republic.
E-mail address: maalidph@yahoo.co.uk.
http://dx.doi.org/10.1016/j.ijhydene.2015.11.127
0360-3199/Copyright © 2015, Hydrogen Energy Publications, LLC. Published by Elsevier Ltd. All rights reserved.

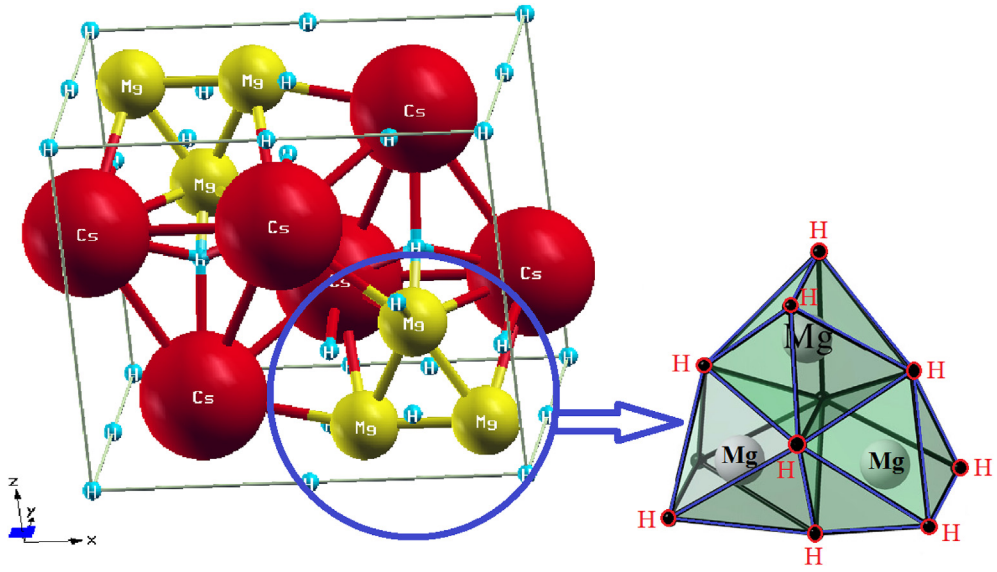

Fig. 1 – The crystal structure of α-$CsMgH_3$. It has been found that α-$CsMgH_3$ consist of $[MgH_6]^{4-}$ octahedrons connected via four corners to 2D-slabs. The building block of α-$CsMgH_3$ is formed by three $[MgH_6]^{4-}$ octahedrons, each of them is condensed into triangular $[3MgH_3]^{3-}$ trimers.

and contains octahedral $[MgH_6]^{-4}$ anions. Several research activities were performed to investigate the suitability and stability of the complex hydrides to be considered as promising hydrogen storage materials [8–12]. The experimental finding state that $CsMgH_3$ occurs in two different modifications, the high pressure trigonal β-$CsMgH_3$ phase [13] and the intermediate pressure orthorhombic α-$CsMgH_3$ phase [9]. The α-phase occur at much lower energy than β-phase [12]. It has been found that α-phase consist of three highly distorted MgH_6 octahedra in each building block, this give α-$CsMgH_3$ superior atomic arrangement among the other Mg-based phases [12]. Therefore, α-$CsMgH_3$ is one of the suitable and stabile materials at moderate pressures and temperatures [9,12]. This motivated us to perform a first principles calculation for α-$CsMgH_3$ phase based on the density functional theory (DFT) to investigate the electronic band structure, total and partial density of states, valence electronic charge density distribution and the chemical bonding characters. Furthermore, deep insight into the electronic band structure can be gained from the optical transitions therefore, we have calculated the optical properties of α-$CsMgH_3$ phase. In such calculation the energy eigenvalues and electron wave functions were involved. Thus, the obtained optical properties are natural outputs of band structure calculations.

As there exists several calculations were performed on the electronic band structure of α-$CsMgH_3$ using different theoretical approaches, non of them have used an accurate exchange correlation potential such like GW approximation [14] or the recently modified Becke–Johnson potential (*mBJ*) [15] to obtain an accurate band splitting and hence accurate band gap's value. One of the powerful method to solve the quantum many body problem is the density functional theory. In this method by using the Kohn–Sham equations we map an interacting many body system to non-interacting hypothetical system which has the same electron density. The price that we will pay is the definition of a new functional that called exchange-correlation functional. Unfortunately exact form of the exchange-correlation functional is unknown. Therefore, the accuracy of DFT results will be sensitive to the selection of the exchange-correlation functional which can play a major role for the accuracy of the results, this is one of the main questions in DFT. Which exchange correlation can accurately describe the properties of the materials.

To the best of our knowledge there is lack information about the optical properties of α-$CsMgH_3$ which can brings deep insight into the electronic structure. Therefore, as a natural extension to the existence information a detailed depiction of the electronic structure, density of states and

Table 1 – Optimized crystal structure in comparison with the experimental data [9] and the previous theoretical calculations [12].

Cell parameters (Å)	a	b	c
Exp.	9.9958 (1)[a]	6.13271 (6)[a]	8.57364 (9)[a]
This work	9.9976	6.13311	8.57413
Previous work	9.9922[b]	6.1405[b]	8.5768[b]

Atomic positions						
Atom	x exp. [a]	x optim.	y exp. [a]	y optim.	z exp. [a]	z optim.
Cs1 (2a)	0.25	0.25	0.25	0.25	0.182 (2)	0.180
Cs2 (4f)	0.476 (1)	0.474	0.25	0.25	0.665 (2)	0.664
Mg1 (2b)	0.25	0.25	0.75	0.75	0.642 (2)	0.640
Mg2 (4f)	0.608 (1)	0.606	0.25	0.25	0.067 (1)	0.065
H1 (2b)	0.25	0.25	0.75	0.75	0.098 (2)	0.094
H2 (4c)	0.0	0.0	0.0	0.0	0.0	0.0
H3 (46)	0.25	0.25	0.990 (2)	0.991	0.494 (1)	0.493
H4 (4e)	0.25	0.25	0.953 (2)	0.950	0.835 (2)	0.833
H5 (4f)	0.550 (1)	0.548	0.25	0.25	0.300 (2)	0.301

[a] Ref. [9].
[b] Ref. [12].

the valence electronic charge density distribution using full potential method within different exchange correlation potentials is timely and would bring us important insights in understanding the origin of the band structure. In addition, we gain more details about the electronic structure through the calculated optical properties. Hence it is very important to use the all-electron full-potential linear augmented plane wave ($FPLAPW + lo$) method to investigate the electronic band structure, density of states, the electron charge density distribution and the optical properties within mBJ. In the recent years due to the improvement of the computational technologies, it has been proven that the first-principles calculation is a strong and useful tool to predict the crystal structure and its properties which are related to the electron configuration of a material before its synthesis [16–19].

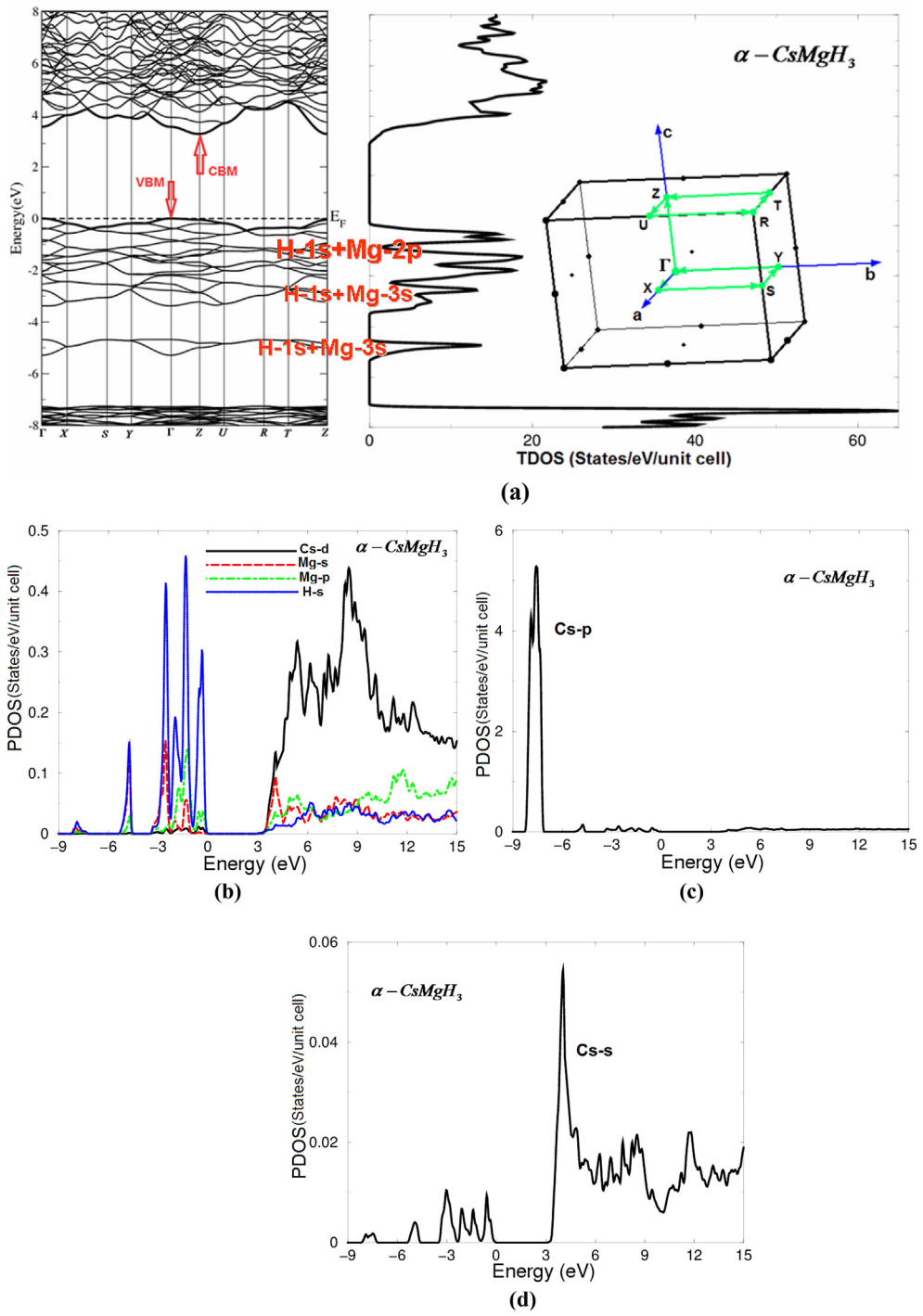

Fig. 2 – (a) Calculated band structure along with the total density of states; (b–d) calculated Cs-6s/5p/4d, Mg-3s/2p and H-1s partial density of states.

Details of calculation

Renaudin et al. [9] have reported that α-$CsMgH_3$ crystallized in orthorhombic symmetry of *Pmmn* (#59) space group. The reported experimental lattice constants are a = 9.9958(1) Å, b = 6.13271(6) Å and c = 8.57364(9) Å [9]. It has been found that α-$CsMgH_3$ consist of $[MgH_6]^{4-}$ octahedrons connected via four corners to 2D-slabs. The building block of α-$CsMgH_3$ is formed by three $[MgH_6]^{4-}$ octahedrons, each of them is condensed into triangular $[3MgH_3]^{3-}$ trimers. The crystal structure of the orthorhombic α-$CsMgH_3$ is shown in Fig. 1. We have used the experimental crystallographic data reported by Renaudin et al. [9] as starting point of this calculations. Using the generalized gradient approximation (*PBE* – GGA) [20] the experimental lattice constants were optimized using the full potential linear augmented plane wave plus local orbitals (*FPLAPW* + *lo*) method as implemented in WIEN2k package [21]. The experimental atomic positions were optimized by minimizing the forces acting on each atom using *PBE* – *GGA*. It has been reported that [20] the *PBE* – *GGA* approach exhibits better equilibrium structural parameters and energetic of different phases therefore, we have used *PBE* – *GGA* for optimized crystal structure. The optimized crystal structure of α-$CsMgH_3$ is presented in Table 1 along with the experimental data [9] and previous theoretical results [12]. From the obtained relaxed geometry the electronic structure, the chemical bonding, electronic charge density and the optical properties have been determined using different exchange-correlation potentials including the recently modified Becke–Johnson potential (*mBJ*). The potential for the construction of basis functions inside the sphere of the muffin tin was

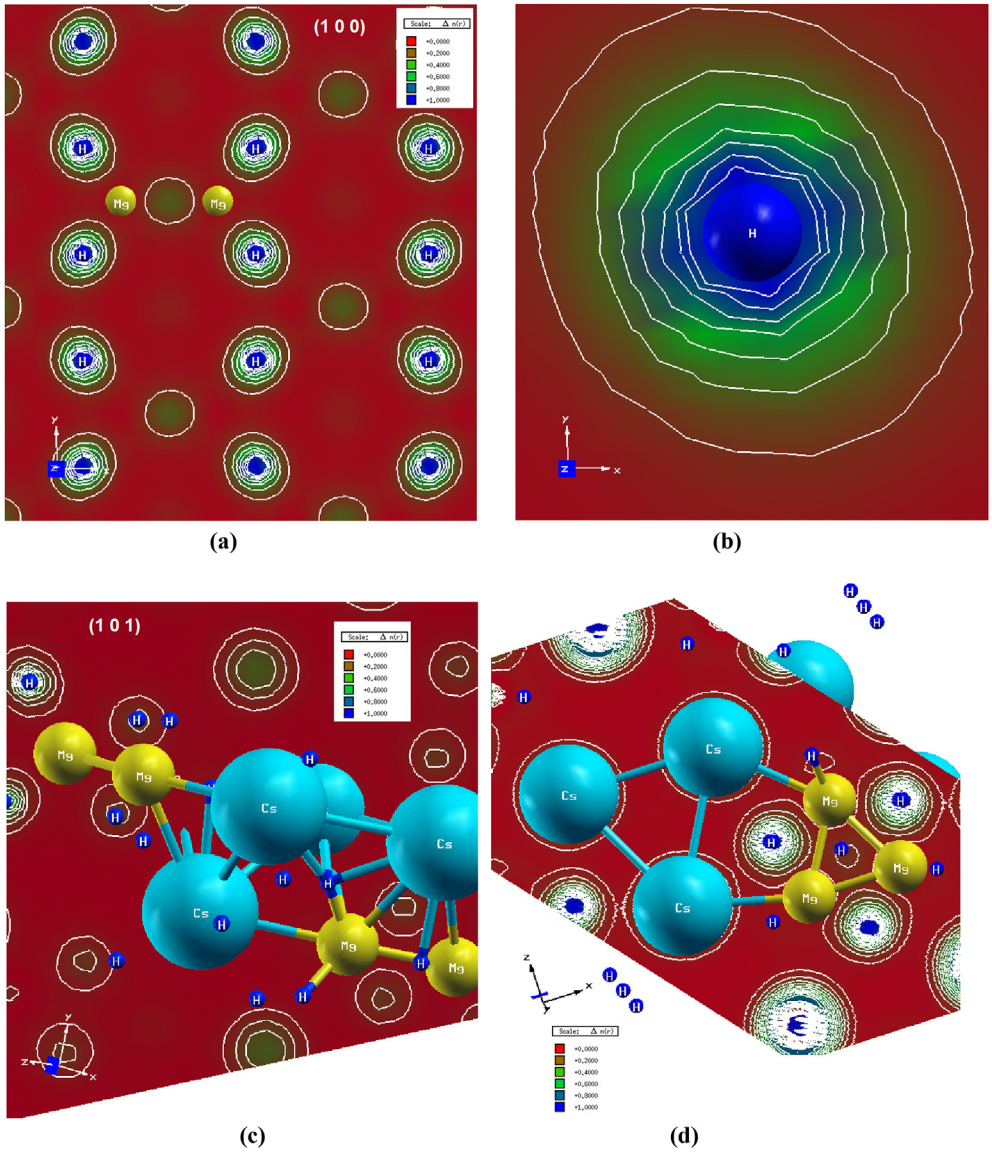

Fig. 3 – (a,c,d) Calculated valence electronic charge density distribution in different crystallographic planes. (b) show the charge transfer towards H atom indicated by the blue color surrounding H atoms, according to thermoscale the blue color indicate the maximum charge accumulation. (For interpretation of the references to color in this figure legend, the reader is referred to the web version of this article.)

spherically symmetric, whereas outside the sphere it was constant [22]. The total and partial density of states (DOS) were calculated by means of the modified tetrahedron method [23]. The input required for calculating the DOS are the energy eigenvalues and eigenfunctions which are the natural outputs of a band structure calculation. The total DOS and partial DOS are calculated for a large energy range (−9.0 eV up to 15.0 eV). The states below the Fermi energy (E_F) are the valence states and states above E_F are the conduction states. Hence we obtain DOS for both valence and conduction band states. Self-consistency is obtained using 200 $\vec{k}$ points in the irreducible Brillouin zone (*IBZ*). The self-consistent calculations are converged since the total energy of the system is stable within 0.00001 R y. The electronic band structure and the related properties were performed within 1000 $\vec{k}$ points in the *IBZ*.

Results and discussion

Electronic band structure, density of states and valence electronic charge density

In order to explore the dispersion of the electronic band structure of the orthorhombic α-$CsMgH_3$, the electronic band structure is calculated using different exchange correlation potentials (XC) so as to obtain the more reliable results. It is well known that the calculation of the energy band gap within DFT is strongly dependent on the approximations used and in particular on the exchange and correlation potential. In order to treat the many-body problems correctly one should go beyond the usual density functional approximations by using GW approximation or the recently modified Becke–Johnson potential (mBJ), which optimizes the corresponding potential for electronic band structure calculations. The modified Becke–Johnson potential allows the calculation with accuracy similar to the very expensive GW calculations [15]. It is a local approximation to an atomic "exact-exchange" potential and a screening term. Based on our experiences on using different exchange-correlation functional (LDA, PBE-GGA, EV-GGA, LDA-mBJ and PBE-GGA-mBJ) on several systems whose energy band gaps are known experimentally. We found that the obtained energy band gap by using PBE-GGA-mBJ show very good agreement with those experimental data [24–26]. Therefore, we chose to show the results obtained by PBE-GGA-mBJ as illustrated in Fig. 2.

We set the zero-point of energy (Fermi level) at the valence band maximum (*VBM*). It has been found that the conduction band minimum (*CBM*) is located at Z point and the *VBM* at Γ point of the first *BZ*. Therefore, α-$CsMgH_3$ exhibit indirect band gap of about 2.3 eV (LDA), 2.6 (PBE-GGA), 2.9 (EVGGA) and 3.2 (PBE-GGA-mBJ) in comparison with the previously calculated energy gap 2.98 eV using VASP-GGA [12], 3.3 eV (Quantum-ESPPRESSO-GGA) [10] and 3.0 eV (VASP-PW91-GGA) [11]. To date, no experimental value for the energy gap is available in the literature to make a meaningful comparison with our theoretical results. Therefore, based on our previous experiences with using mBJ, we expected the obtained *mBJ*-gap is closer to the expected measured one. Future experimental work will testify our calculated results.

To carefully investigate the role of the orbitals of each atom, we have explored the angular momentum projected density of states. In Fig. 2(a) we illustrated the calculated total density of states (*TDOS*) obtained by *mBJ* which confirm the values of the energy gap of about 3.2 eV and the dispersions of the orbitals below and above Fermi level (E_F). The angular momentum character of the various structures for α-$CsMgH_3$ were obtained from calculating the angular momentum projected density of states (*PDOS*) as shown in Fig. 2(b–d). The structures below E_F are mainly originated from H-1s and Mg-3s/2p states with small contribution from Cs-6s/5p/4d states. While the structures from CBM and above are originated from Cs-4d with small contribution from Mg-3s/2p, H-1s and Cs-6s states. It has been noticed that Mg-3s/2p state hybridized with H-1s state above and below E_F.

From the electronic band structure and the TDOS we can see that at the energy regions around −5.0 eV and from −3.5 eV up to −2.0 eV the H-1s state hybridized with Mg-3s state to form a peak at around −5.0 eV and three peaks from −3.5 eV up to −2.0 eV in the TDOS plot. The energy

Table 2 – Selected bond lengths in comparison with the experimental data [9].

Bonds	Bond lengths (this work)	Bond lengths (Exp.)	Bonds	Bond lengths (this work)	Bond lengths (Exp.)
Cs1-H3	3.109	3.11 (2)	Mg2-H4	2.055	2.06 (1)
Cs1-H1	3.137	3.145 (6)	Mg2-H5	2.076	2.08 (2)
Cs1-H5	3.159	3.16 (1)	Mg1-Mg2	2.811	2.87 (2)
Cs1-H2	3.301	3.31 (1)	Mg2-Mg2	2.804	2.84 (2)
Cs1-H4	3.472	3.48 (2)	H1-H4	2.567	2.57 (2)
Cs2-H5	3.083	3.086 (2)	H1-H2	3.041	3.043 (4)
Cs2-H3	3.118	3.12 (1)	H4-H4	3.478	2.49 (1)
Cs2-H4	3.235	3.24 (1)	H4-H5	2.601	2.62 (1)
Cs2-H2	3.254	3.26 (1)	H4-H2	2.871	2.878 (8)
Mg1-H3	1.931	1.94 (2)	H4-H3	2.916	2.93 (2)
Mg1-H5	2.057	2.06 (1)	H2-H5	3.028	3.03 (1)
Mg1-H4	2.066	2.07 (2)	H2-H2	3.058	3.0611 (1)
Mg2-H2	1.911	1.955 (8)	H3-H3	2.911	2.94 (2)
Mg2-H1	2.01	2.00 (1)	H5-H3	4.036	3.04 (1)

Exp. Ref. [9].

region from −2.0 eV up to E_F is originated by the interactions between H-1s and Mg-2p states. Thus, the interactions between the orbitals of H and Mg atoms leads to form strong covalent bonding between H and Mg atoms. Covalent bonding is more favorable for the transport of the carriers than ionic one [27]. The conduction bands are mainly originated from the empty states of Cs and partially from Mg-3s/2p states while H-1s has insignificant contribution to the empty states.

Further, we can use the angular momentum decomposition of the atoms projected electronic density of states to elucidate the characters of chemical bonding. In the energy region extended between −9.0 eV and Fermi level we can obtain the total number of electrons/eV (*e*/*eV*) for the orbitals in α-$CsMgH_3$ compound as follow, H-1s state 4.6 *e*/*eV*, Mg-3s state 1.5 *e*/*eV* and Mg-2p state 1.5 *e*/*eV*. The contributions of H-1s, Mg-3s/2p orbitals to the VBs exhibit that there are some electrons from Mg and H atoms are transferred into VBs and contribute in covalence interactions between the atoms. The strength/weakness of the covalent bonding arises due to the degree of the hybridization and the electronegativity differences between Mg and H atoms. Thus, the interaction of charges between Mg and H atoms exhibit strong covalent bonding.

For deep analyzing to the electronic structure we have calculated the valence band's electronic charge density distribution in two crystallographic planes as shown in Fig. 3(a)–(c). This can give clear image of the electronic charge surrounding the atoms and the charge transfer which can help to identify the bonding features. The crystallographic plane in the (100) direction show that the H atoms are surrounding by uniform spherical charge. The Pauling electronegativity of Cs, Mg and H atoms are 0.79, 1.31 and 2.20, respectively. Thus, according to the electronegativity difference between the atoms, charge transfer occurs toward H atoms as shown by the maximum charge surrounding H atoms (see Fig. 3(b)). According to thermoscale the blue color indicate the maximum charge accumulation. In addition we have calculated the crystallographic plane in the direction (101) as shown in Fig. 3(c), which confirm our previous observation that the characters of the H–Mg bonds are mostly ionic and partially covalent. Fig. 3(d) reveals that the Cs atom form ionic bonding with H atom and a charge transfer occurs toward H atoms. We have calculated the bond lengths as shown in Table 2 in comparison with the experimental data [9], good agreement was found.

Optical response

Deep insight into the electronic band structure can be obtained from calculating the optical properties of the materials. Therefore, as step forward to understanding the electronic band structure of α-$CsMgH_3$ we have performed details description for the frequency dependent dielectric functions. It is well-know that calculations of the dielectric functions involve the energy eigenvalues and electron wave functions. These are natural outputs of band structure calculations. Hence, a clear picture can be gained from the optical transitions which mapped the band dispersions according to the dipolar selection rule, which state that only transitions changing the angular momentum quantum number *l* by unity ($\Delta = \pm 1$) are allowed. Since α-$CsMgH_3$ possess orthorhombic symmetry so there are only three non-zero components of the dielectric tensor. These are corresponding to an electric field perpendicular and parallel to the c-axis. The complex dielectric function $\varepsilon(\omega) = \varepsilon_1(\omega) + i\varepsilon_2(\omega)$ is well explained the optical properties of materials. The imaginary part $\varepsilon_2^{xx}(\omega)$, $\varepsilon_2^{yy}(\omega)$ and $\varepsilon_2^{zz}(\omega)$ can be obtained following the expression [28].

$$\varepsilon_2(\omega) = \frac{8}{3\pi\omega^2}\sum_{nn'}\int_{BZ}|P_{nn'}(k)|^2\frac{dS_k}{\nabla\omega_{nn'}(k)} \quad (1)$$

where $P_{nn'}(k)$ is the dipolar matrix elements between initial $|nk\rangle$ and final $|n'k\rangle$ states with their eigenvalues $E_n(k)$ and $E_{n'}(k)$, respectively. $\omega_{nn'}(k)$ is the inter-band energy difference.

$$\omega_{nn'}(k) = E_n(k) - E_{n'}(k) \quad (2)$$

whereas the real part can be obtained from the imaginary part with the aid of Kramers–Kronig relations [29,30].

$$\varepsilon_1(\omega) = 1 + \frac{2}{\pi}P\int_0^\infty \frac{\omega'\varepsilon_2(\omega')}{\omega'^2 - \omega^2}d\omega' \quad (3)$$

where p implies the principle value of the integral.

In Fig. 4(a) we illustrated the imaginary and real parts of the frequency-dependent optical dielectric functions obtained by using *mBJ* approach. The imaginary part reveals that the absorption edges of $\varepsilon_2^{xx}(\omega)$, $\varepsilon_2^{yy}(\omega)$ and $\varepsilon_2^{zz}(\omega)$ occurs at 3.2 eV. Therefore, from the imaginary part dispersions we can directly obtain the energy band value. While indirectly from the real part following Penn model $\varepsilon(0) \approx 1 + (\hbar\omega_P/E_g)^2$ [31]. Penn proposed a relation between $\varepsilon(0)$ and E_g, E_g is some kind of averaged energy gap which could be related to the real energy gap. The calculated values of $\varepsilon_1^{xx}(0)$, $\varepsilon_1^{yy}(0)$ and $\varepsilon_1^{zz}(0)$ along with the calculated energy band gap and the plasmon oscillations ω_p^{xx}, ω_p^{yy} and ω_p^{zz} are listed in Table 3. The later are associated with inter-band transitions. The plasmon maximum is usually the most intense feature in the spectrum and this is at energy where $\varepsilon_1^{xx}(\omega)$, $\varepsilon_1^{yy}(\omega)$ and$\varepsilon_1^{zz}(\omega)$ crosses zero which is associated with the existence of plasma oscillations. The uniaxial anisotropy ($\delta\varepsilon$) can be obtained from $\varepsilon_1^{xx}(0)$, $\varepsilon_1^{yy}(0)$ and $\varepsilon_1^{zz}(0)$. It has been found that α-$CsMgH_3$ possess positive $\delta\varepsilon$ (Table 3) which reveals that α-$CsMgH_3$ exhibit isotropic nature at low energies. Further analyzing to the electronic structure can be obtained from the imaginary part, the observed absorption edges occurs due to the transition from H-1s and Mg-2p states in the VBs to the Cs-6s/4d Mg-3s in the CBs. The main peaks of the imaginary part which are situated at around 5.2 eV is originated due to the transition from H-1s and Mg-3s states of the VBs to Cs-6s/4d, Mg-3s/2p and H-1s states of the CBs. The tail is formed due to Cs-5p, H-1s and Mg-3s (VBs) to Cd-6s/4d, Mg-3s/2p and H-1s states (CBs). To reveals the origin of the spectral structures of $\varepsilon_2^{xx}(\omega)$, $\varepsilon_2^{yy}(\omega)$ and$\varepsilon_2^{zz}(\omega)$, we have used our calculated band structure to indicate the transitions which are responsible for the major structure of $\varepsilon_2^{xx}(\omega)$, $\varepsilon_2^{yy}(\omega)$ and$\varepsilon_2^{zz}(\omega)$. These transitions are labeled according to the spectral peak positions in Fig. 4(a). For simplicity, we have labeled the transitions in Fig. 4(a) and (b), as A, B, and C. The transitions (A) are responsible for the structures for $\varepsilon_2^{xx}(\omega)$, $\varepsilon_2^{yy}(\omega)$ and$\varepsilon_2^{zz}(\omega)$ in the

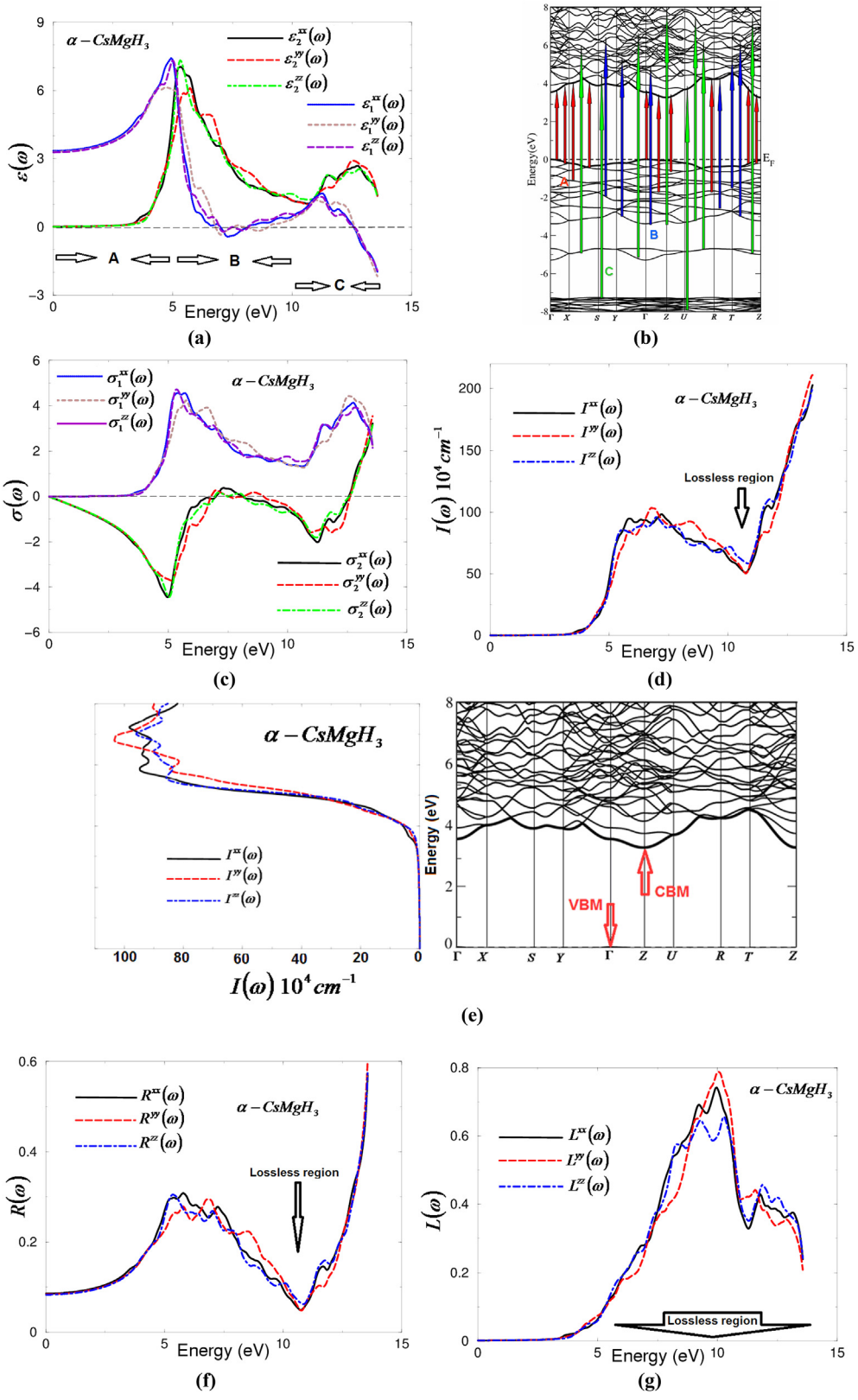

Fig. 4 – (a) Calculated $\varepsilon_2^{xx}(\omega)$ (dark solid curve – black color online), $\varepsilon_2^{yy}(\omega)$ (light long dashed curve – red color online) and $\varepsilon_2^{zz}(\omega)$ (light dotted dashed curve – green color online) along with Calculated $\varepsilon_1^{xx}(\omega)$ (dark solid curve – blue color online), $\varepsilon_1^{yy}(\omega)$ (light dashed curve – brown color online) and $\varepsilon_1^{zz}(\omega)$ (light sold curve – violet color online); (b) The optical transitions depicted on a generic band structure of α-$CsMgH_3$. For simplicity, we have labeled the optical transitions as A, B, and C. The transitions (A) are responsible for the structures for $\varepsilon_2^{xx}(\omega)$, $\varepsilon_2^{yy}(\omega)$ and $\varepsilon_2^{zz}(\omega)$ in the spectral range 0.0–5.0 eV; the transitions (B) 5.0–10.0 eV, and the transitions (C) 10.0–14.0 eV; (c) Calculated $\sigma_2^{xx}(\omega)$ (dark solid curve – black color online), $\sigma_2^{yy}(\omega)$ (light dashed curve –

Table 3 – The calculated energy band gap in comparison with the previous calculation [10–12], $\varepsilon_1^{xx}(0)$, $\varepsilon_1^{yy}(0)$, $\varepsilon_1^{zz}(0)$, $\delta\varepsilon$, ω_p^{xx}, ω_p^{yy}, ω_p^{zz}. These parameters are calculated within mBJ.

α-$CsMgH_3$	
Eg (eV)	2.3 (LDA) 2.6 (PBE-GGA), 2.9 (EVGGA) 3.2 (mBJ) 2.98[a], 3.3[b], 3.0[c]
$\varepsilon_1^{xx}(0)$	3.350
$\varepsilon_1^{yy}(0)$	3.307
$\varepsilon_1^{zz}(0)$	3.285
$\delta\varepsilon$	0.016
ω_p^{xx}	7.006
ω_p^{yy}	6.816
ω_p^{zz}	6.979

[a] Ref. [12] 2.98 eV using VASP-GGA.
[b] Ref. [10] 3.3 eV (Quantum-ESPPRESSO-GGA).
[c] Ref. [11] 3.0 eV (VASP-PW91-GGA).

spectral range 0.0–5.0 eV, the transitions (B) 5.0–10.0 eV, and the transitions (C) 10.0–14.0 eV. Thus the calculated imaginary part of the optical dielectric functions helps to analyze the orbitals dispersions.

In order to gain further understanding of the electronic structure, the optical conductivity $\sigma_2(\omega)$ and $\sigma_1(\omega)$ are calculated as shown in Fig. 4(c). These are directly related to the complex dielectric function $\varepsilon(\omega) = \varepsilon_1(\omega) + i\varepsilon_2(\omega)$. It is clear that the imaginary part $\sigma_2^{xx}(\omega)$, $\sigma_2^{yy}(\omega)$ and $\sigma_2^{zz}(\omega)$ confined in the energy region between 0.0 and the values of ω_p^{xx}, ω_p^{yy} and ω_p^{zz} exhibit overturned features of $\varepsilon_2^{xx}(\omega)$, $\varepsilon_2^{yy}(\omega)$ and $\varepsilon_2^{zz}(\omega)$, whereas the real parts $\sigma_1^{xx}(\omega)$, $\sigma_1^{yy}(\omega)$ and $\sigma_1^{zz}(\omega)$ show similar features to that of $\varepsilon_2^{xx}(\omega)$, $\varepsilon_2^{yy}(\omega)$ and $\varepsilon_2^{zz}(\omega)$. The absorption spectra as shown in Fig. 4(d) reveals that there exists four spectral regions, the obscure regain (below the energy gap), intermediate absorption region (3.2 up to 9.0 eV), lossless region (9.0 up to 11.5 eV) and high absorption region (11.5 eV and above). The observed lossless region confirms the occurrence of a collective plasmon resonance (ω_P). We should emphasize that above ω_P the material behaves as dielectric where $\varepsilon_1(\omega)$ is positive, while below ω_P where $\varepsilon_1(\omega)$ is negative the material exhibit metallic nature.

Fig. 4(e) reveals the origin of the absorption edges associated to the electronic band structure. It is clear that α-$CsMgH_3$ compound posses wide optical transparency region up to 3.2 eV (λ = 3874.5 Å). The calculated optical reflectivity spectra (Fig. 4(f)) explore the occurrence of a collective plasmon resonance, the region where the values of plasma resonance situated in concordance with our observation in Fig. 4(a,c–e). The calculated loss function (Fig. 4(g)) as a function to photon energy exhibits that there exists a strong lossless region between 9.0 eV and 11.5 eV in concordance with Fig. 4(a,c–f). The loss function's peaks represent ω_P and hence the lossless region.

Conclusions

We have reported comprehensive theoretical calculations for α-$CsMgH_3$ using the full potential method so as to understand the suitability and stability of using α-$CsMgH_3$ as hydrogen storage materials. The experimental geometrical structure is optimized by using $PBE-GGA$ approach. The calculated electronic band structure reveals that α-$CsMgH_3$ has indirect energy band gap. It has been found that the value of the obtained band gap is about 2.3 eV (LDA), 2.6 (PBE-GGA), 2.9 (EVGGA) and 3.2 (PBE-GGA-mBJ) in comparison with the previously calculated energy gap 2.98 eV using VASP-GGA, 3.3 eV (Quantum-ESPPRESSO-GGA) and 3.0 eV (VASP-PW91-GGA). The calculated angular momentum projected density of states explore that there exists strong hybridization between H-1s and Mg-3s/2p states which reveals the existence of the covalent bonding. The calculated bond distance agree well with the measured one. The calculated valence band's electronic charge density explore the covalent nature of Mg–H bonds and the ionic nature of Cs–H bonds. In addition, the valence band's electronic charge density reveals the occurrence of charge transfer towards H atoms. The calculated optical properties gave deep insight into the electronic structures so as further understanding to the atomic arrangement can be obtained. The absorption coefficient confirm the energy gap's value and the positive uniaxial anisotropy reveals that α-$CsMgH_3$ exhibit isotropic nature at low energies.

Acknowledgments

The result was developed within the CENTEM project, reg. no. CZ.1.05/2.1.00/03.0088, cofunded by the ERDF as part of the Ministry of Education, Youth and Sports OP RDI programme and, in the follow-up sustainability stage, supported through CENTEM PLUS (LO1402) by financial means from the Ministry of Education, Youth and Sports under the "National

red color online) and $\sigma_2^{zz}(\omega)$ (light dotted dashed curve – green color online) along with Calculated $\sigma_1^{xx}(\omega)$ (dark solid curve – blue color online), $\sigma_1^{yy}(\omega)$ (light dashed curve – red brown online) and $\sigma_1^{zz}(\omega)$ (light solid curve – violet color online) for α-$CsMgH_3$; (d) Calculated absorption coefficient $I^{xx}(\omega)$ (dark solid curve – black color online), $I^{yy}(\omega)$ (light dashed curve – red color online) and $I^{zz}(\omega)$ (light dotted dashed curve – blue color online) spectrum for α-$CsMgH_3$ the absorption coefficient in 10^4 cm^{-1}; (e) Calculated absorption coefficient $I^{xx}(\omega)$ (dark solid curve – black color online), $I^{yy}(\omega)$ (light dashed curve – red color online) and $I^{zz}(\omega)$ (light dotted dashed curve – blue color online) spectrum for α-$CsMgH_3$ the absorption coefficient in 10^4 cm^{-1} at the energy range between 0 and 8.0 eV along with the electronic band structure at the energy range between 0 and 8.0 eV; (f) Calculated $R^{xx}(\omega)$ (dark solid curve – black color online), $R^{yy}(\omega)$ (light dashed curve – red color online), and $R^{zz}(\omega)$ (light dotted dashed curve – blue color online) for α-$CsMgH_3$; (g) Calculated absorption coefficient $L^{xx}(\omega)$ (dark solid curve – black color online), $L^{yy}(\omega)$ (light dashed curve – red color online) and $L^{zz}(\omega)$ (light dotted dashed curve – blue color online) spectrum for α-$CsMgH_3$. (For interpretation of the references to color in this figure legend, the reader is referred to the web version of this article.)

Sustainability Programme I. Computational resources were provided by MetaCentrum (LM2010005) and CERIT-SC (CZ.1.05/3.2.00/08.0144) infrastructures.

REFERENCES

[1] Block J, Gray AP. The thermal decomposition of lithium aluminum hydride. Inorg Chem 1965;304:4.
[2] Dilts JA, Ashby EC. Thermal decomposition of complex metal hydrides. Inorg Chem 1972;11:1230.
[3] Bogdanovic B, Schwickardi M. Ti-doped alkali metal aluminium hydrides as potential novel reversible hydrogen storage materials. J Alloys Compd 1997;253–255:1.
[4] Bogdanovic B, Brand RA, Marjanovic A, Schwikardi M, Tolle J. Metal-doped sodium aluminium hydrides as potential new hydrogen storage materials. J Alloys Compd 2000;302:36.
[5] Brinks HW, Hauback BC, Norby P, Fjellvag H. The decomposition of $LiAlD_4$ studied by in-situ X-ray and neutron diffraction. J Alloys Compd 2003;351:222.
[6] Jensen CM, Gross K. Development of catalytically enhanced sodium aluminum hydride as a hydrogen storage material. J Appl Phys A 2001;72:213.
[7] Morioka H, Kakizaki K, Chung SC, Yamada A. Reversible hydrogen decomposition of $KAlH_4$. J Alloys Compd 2003;353:310.
[8] Yvon K, Bertheville B. Magnesium based ternary metal hydrides containing alkali and alkaline-earth elements. J Alloys Compd 2006;425:101–8.
[9] Renaudin G, Bertheville B, Yvon K. Synthesis and structure of an orthorhombic low-pressure polymorph of caesium magnesium hydride, $CsMgH_3$. J Alloys Compd 2003;353:175–9.
[10] An P, Li Y, Xu Y, Cui T, Wang H, Li Y, et al. Electronic and optical properties of orthorhombic and hexagonal phases of $CsMgH_3$: first-principles calculations. Phys B 2009;404:1061–9.
[11] Wang Z, Wang Y, Tang B, Zeng X, Ding W. Theoretical study of the $CsMgH_3$, Cs_2MgH_4 and $Cs_4Mg_3H_{10}$ complex hydrides from first-principles. Phys Stat Sol B 2008;245:2749–55.
[12] Vajeeston P, Ravindran P, Kjekshus A, Fjellvag H. First-principles investigations of the $MMgH_3$ (M-Li, Na, K, Rb, Cs) series. J Alloys Compd 2008;450:327–37.
[13] Bertheville B, Fischer P, Yvon K. High-pressure synthesis and crystal structures of new ternary caesium magnesium hydrides, $CsMgH_3$, $Cs_4Mg_3H_{10}$ and Cs_2MgH_4. J Alloys Compd 2002;330–332:152–6.
[14] Gygi F, Baldereschi A. Quasiparticle energies in semiconductors: self-energy correction to the local-density approximation. Phys Rev Lett 1989;62:2160.
[15] Tran F, Blaha P. Accurate band gaps of semiconductors and insulators with a semilocal exchange-correlation potential. Phys Rev Lett 2009;102 226401.
[16] Plucinski KJ, Kityk IV, Kasperczyk J, Sahraoui B. The structure and electronic properties of silicon oxynitride gate dielectrics. Semicond Sci Technol 2001;16:467–70.
[17] Malachowski M, Kityk IR, Sahraoui B. Electronic structure and optical response in $Ga_xAl_{1-x}N$ solid alloys. Phys Lett A 1998;242:337–42.
[18] Fuks-Janczarek I, Miedzinski R, Brik MG, Majchrowski A, Jaroszewicz LR, Kityk IV. Z-scan analysis and ab initio studies of beta-$BaTeMo_2O_9$ single crystal. Solid State Sci 2014;27:30–5.
[19] Ma C-G, Brik MG. First principles studies of the structural, electronic and optical properties of $LiInSe_2$ and $LiInTe_2$ chalcopyrite crystals. Solid State Commun 2015;203:69–74.
[20] Perdew JP, Burke S, Ernzerhof M. Generalized gradient approximation made simple. Phys Rev Lett 1996;77:3865.
[21] Blaha P, Schwarz K, Madsen GKH, Kvasnicka D, Luitz J. WIEN2k, an augmented plane wave plus local orbitals program for calculating crystal properties. Austria: Vienna University of Technology; 2001.
[22] Schwarz K, Blaha P. Solid state calculations using WIEN2k. Comput Mater Sci 2003;28:259.
[23] Blöchl PE, Jepsen O, Andersen OK. Improved tetrahedron method for Brillouin-zone integrations. Phys Rev B Condens Matter 1994;15;49(23):16223–33.
[24] Reshak AH. Specific features of electronic structures and optical susceptibilities of molybdenum oxide. RSC Adv 2015;5:22044.
[25] Reshak AH, Huang Hongwei, Kamarudin H, Auluck S. Alkali-metal/alkaline-earth-metal fluorine beryllium borate $NaSr_3Be_3B_3O_9F_4$ with large nonlinear optical properties in the deep-ultraviolet region. J Appl Phys 2015;117:085703.
[26] Reshak AH. Transport properties of g-BC_3 and t-BC_3 phases. RSC Adv 2015;5:33632.
[27] Wu F, Song HZ, Jia JF, Hu X. Effects of Ce, Y, and Sm doping on the thermoelectric properties of Bi_2Te_3 alloy. In: Progress in natural science: materials international23; 2013. p. 408–12.
[28] Khan MA, Kashyap Arti, Solanki AK, Nautiyal T, Auluck S. Interband optical properties of Ni_3Al. Phys Rev B 1993;23:16974.
[29] Hufner S, Claessen R, Reinert F, Straub Th, Strocov VN, Steiner P. Photoemission spectroscopy in metals: band structure— Fermi surface—spectral function. J Electron Spectra Relat Phenom 1999;100:191–213.
[30] Wooten F. Optical properties of solids. New York and London: Academic Press; 1972.
[31] Penn DR. Wave-number-dependent dielectric function of semiconductors. Phys Rev B 1962;128:2093.